

Article

Cooperative Ternary Assemblies Involving Anion- π / π - π /Anion- π Assemblies and Unconventional Cl \cdots Cl Interactions in Cu(II) Coordination Compounds: Experimental and Theoretical Studies

Pinku Sarma¹, Rosa M. Gomila², Antonio Frontera^{2,*}, Miquel Barcelo-Oliver²
and Manjit K. Bhattacharyya^{1,*}

¹ Department of Chemistry, Cotton University, Guwahati 781001, India

² Departament de Química, Universitat de les Illes Balears, Crta de Valldemossa km 7.7, 07122 Palma de Mallorca, Balears, Spain

* Correspondence: toni.frontera@uib.es (A.F.); manjit.bhattacharyya@cottonuniversity.ac.in (M.K.B.)

Abstract: Two coordination compounds of Cu(II), namely, [Cu(phen)₂Cl](NO₃)·H₂O (compound 1) and [Cu₂(μ -Cl₂)Cl₂(Hdmpz)₄] (compound 2), where phen = 1,10-phenanthroline and Hdmpz = 3,5-dimethylpyrazole, were synthesized at room temperature and characterized using elemental analysis, TGA, spectroscopic techniques (FT-IR and electronic) and single-crystal X-ray diffraction studies. The cooperative anion- π / π - π /anion- π assemblies involving the coordinated phen, along with the uncoordinated nitrate moieties, played pivotal roles in the stabilization of the crystal structure of compound 1. Unconventional type I Cl \cdots Cl interactions involving the coordinated Cl atoms provided reinforcement to the crystal structure of compound 2. We theoretically explored the supramolecular assemblies observed in the crystal structures of compounds 1 and 2 using DFT calculations, MEP surface analysis and combined NCI plot/QTAIM computational tools. Theoretical analysis revealed that the antiparallel π -stacking interactions in compound 1 and the N-H \cdots Cl H-bonds in compound 2 were the strong structure-guiding non-covalent synthons which stabilized the compounds. In the anion- π / π - π /anion- π assembly observed in compound 1, the anion- π interaction reinforced the π -stacking by reducing the electrostatic repulsion between the metal-coordinated electron-deficient phen rings.

Keywords: coordination compound; cooperative assemblies; Cl \cdots Cl interaction; DFT calculations; NCI plot/QTAIM analysis



Citation: Sarma, P.; Gomila, R.M.; Frontera, A.; Barcelo-Oliver, M.; Bhattacharyya, M.K. Cooperative Ternary Assemblies Involving Anion- π / π - π /Anion- π Assemblies and Unconventional Cl \cdots Cl Interactions in Cu(II) Coordination Compounds: Experimental and Theoretical Studies. *Crystals* **2023**, *13*, 517. <https://doi.org/10.3390/cryst13030517>

Academic Editor: Slawomir Grabowski

Received: 8 February 2023

Revised: 11 March 2023

Accepted: 13 March 2023

Published: 17 March 2023



Copyright: © 2023 by the authors. Licensee MDPI, Basel, Switzerland. This article is an open access article distributed under the terms and conditions of the Creative Commons Attribution (CC BY) license (<https://creativecommons.org/licenses/by/4.0/>).

1. Introduction

The design, synthesis and development of coordination complexes of transition metals have attracted significant attention from researchers not only due to their myriad potential applications in various fields but also due to their intriguing structural topologies [1–4]. Organization of the molecular building blocks via a self-assembly process plays a decisive role in the structural topology and network architectures of coordination compounds [5,6]. However, it is challenging to develop network architectures of the desired dimensionalities as various synthetic factors such as the coordination behavior of the metal centers, organic moieties as ligands, pH, temperature, etc. can effectively influence the design and synthesis of the desired structural topologies [7–9]. The choice of solvent also plays a crucial role in the design of coordination compounds with fascinating network architectures, as solvent molecules can coordinate with the metal centers and/or are present in the crystal lattices, facilitating diverse structural topologies [10,11].

Supramolecular chemistry deals with the non-covalent interactions that play decisive roles in various processes such as in synthetic chemistry, catalysis, the development of

pharmaceutical agents, molecular biology, etc. [12–14]. Myriad attempts have been made in recent times to quantify the self-assembly of non-covalent interactions in coordination compounds [15–19]. Among the various non-covalent interactions, hydrogen-bonding interactions are considered as the most common non-covalent interaction [20]. Coordination compounds involving aromatic ligands are of particular interest in supramolecular chemistry as the aromatic rings can facilitate the π -stacking interactions that play a crucial role in the structural topologies of metal–organic compounds [21,22]. Aromatic π -stacking interactions are also involved in the self-assembly of bio-molecules, namely, the stabilization of DNA's helix structure [23,24], the interactions of drugs/compounds with proteins, etc. [25]. Non-covalent interactions involving anions with electron-deficient aromatics, namely, anion– π interactions, also contribute to the solid state stabilities of supramolecular architectures [26]. The cooperative interplay of non-covalent interactions has also received remarkable emphasis from a crystal engineering viewpoint [27,28]. Unusual non-covalent interactions such as dihydrogen bonding, halogen bonding, etc. also play critical roles in the organization of the structures of the compounds in a solid state, which can also affect the properties of the compounds [29–33]. Unconventional Cl \cdots Cl contacts have also received significant attention in supramolecular chemistry, which can also be considered as donor–acceptor interactions [34]. Usually, the intermolecular C–X1 \cdots X2–C interactions (where X = F, Cl, Br or I), depending on the angles, are of the following two types: $\theta_1 = \angle\text{C-X1}\cdots\text{X2}$ and $\theta_2 = \angle\text{X1}\cdots\text{X2-C}$. The interactions with $\theta_1 = \theta_2$ are called type I, whereas the condition $\theta_1 \neq \theta_2$ belongs to the interactions of type II [35]. Various research groups have already established the donor–acceptor behavior of halogen \cdots halogen interactions using computational studies [36,37]. The uncoordinated anions present in the crystal lattice primarily compensate the overall positive charges of the complex cationic moieties; however, they can also facilitate unusual non-covalent interactions [38,39].

1,10-Phenanthroline (phen), a classic bidentate chelating N-donor moiety, is capable of interacting with various biological systems both as a free ligand and as a coordinated complex to the metal centers [40]. Phen is capable of forming stable coordination complexes with most of the transition metal centers, thereby holding a peculiar place as starting building block in coordination chemistry [41–46]. The presence of electron-deficient aromatic systems in phen makes it an excellent electron acceptor capable of stabilizing metal complexes via various unusual non-covalent interactions [44]. Pyrazole and substituted derivatives and aromatic heterocycles have been extensively used to construct transition metal compounds [47–49]. Both phen and Hdmpz, which are N-donor heterocycles, can be effectively used as building blocks to develop coordination compounds of the desired dimensionalities, with potential applications [50–53].

In the present study, we have reported the synthesis and crystal structures of two coordination compounds of Cu(II), namely, [Cu(phen) $_2$ Cl](NO $_3$) \cdot H $_2$ O (compound **1**) and [Cu $_2$ (μ -Cl $_2$)Cl $_2$ (Hdmpz) $_4$] (compound **2**), where phen = 1,10-phenanthroline and Hdmpz = 3,5-dimethylpyrazole). We have further characterized the compounds using various spectroscopic and analytical techniques such as elemental analysis, TGA and spectroscopic (FT-IR and electronic) techniques. The uncoordinated nitrate anion and water molecule, along with the aromatic π -stacking involving the coordinated phen moieties, stabilized the crystal structure of compound **1**. Unusual type I Cl \cdots Cl contacts involving the coordinated Cl atoms provided stability to the crystal structure of compound **2**. The energetic features of the unconventional non-covalent interactions observed in the compounds have been explored using theoretical studies, with special attention devoted to the anion– π /(π – π)/anion– π ternary assemblies in compound **1** and the N–H \cdots Cl H bonds in compound **2**. The supramolecular assemblies have been theoretically established using molecular electrostatic potential (MEP) surface analysis and the combined QTAIM/NCI plot computational method.

2. Experimental Section

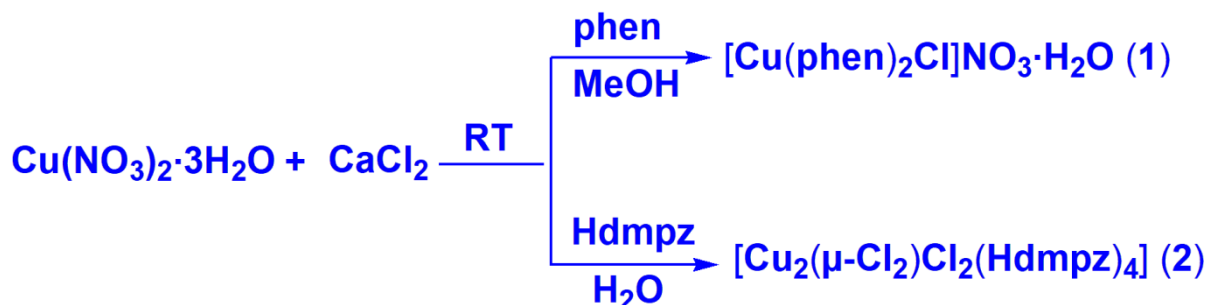
2.1. Materials and Methods

The chemicals used in the present study were purchased from commercial sources and used as received. Elemental analyses of the compounds were carried out using a Perkin Elmer 2400 Series II CHN/O analyzer. A Bruker ALPHA II Infrared spectrophotometer was used to record the FT-IR spectra of the compounds in the frequency range of 4000–500 cm^{-1} . The diffuse-reflectance electronic spectra of the compounds were recorded using a Shimadzu UV-2600 spectrophotometer. To record the solid state UV-Vis-NIR spectra of the compounds, BaSO_4 powder was used as a reference (100% reflectance). Room temperature magnetic moments were calculated at 300 K using a Sherwood Mark 1 Magnetic Susceptibility balance. Thermal analyses of the compounds were carried out with a Mettler Toledo TGA/DSC1 STAR^e system under the flow of N_2 gas at a heating rate of 10 $^\circ\text{C}$ per min^{-1} .

2.2. Syntheses

2.2.1. Synthesis of $[\text{Cu}(\text{phen})_2\text{Cl}]\text{NO}_3 \cdot \text{H}_2\text{O}$ (Compound 1)

$\text{Cu}(\text{NO}_3)_2 \cdot 3\text{H}_2\text{O}$ (0.241 g, 1 mmol) and $\text{CaCl}_2 \cdot 2\text{H}_2\text{O}$ (0.147 g, 1 mmol) were dissolved in 10 mL of methanol and mechanically stirred at room temperature for two hours. To the resulting solution, phen (0.396 g, 2 mmol) was added, and the solution was stirred for another hour (Scheme 1). The resulting solution was kept in cool conditions in a refrigerator for crystallization, from which blue block-shaped crystals were obtained after a few days. The yield was: 0.453 g (84%). The analytically calculated for the $\text{C}_{24}\text{H}_{18}\text{ClCuN}_5\text{O}_4$ were: C, 53.44%; H, 3.36%; and N, 12.98%. We found: C, 53.38%; H, 3.25%; and N, 12.90%. The FT-IR spectral data (KBr disc, cm^{-1}) were: 3452(s), 2825(w), 1588(s), 1427(s), 1382(s), 1374(s), 1351(m), 1145(w), 847(m), 718(m), and 580(w) (where: s, strong; m, medium; w, weak; br, broad; and sh, shoulder).



Scheme 1. Syntheses of compounds 1 and 2.

2.2.2. Synthesis of $[\text{Cu}_2(\mu\text{-Cl}_2)\text{Cl}_2(\text{Hdmpz})_4]$ (Compound 2)

$\text{Cu}(\text{NO}_3)_2 \cdot 3\text{H}_2\text{O}$ (0.241 g, 1 mmol) and $\text{CaCl}_2 \cdot 2\text{H}_2\text{O}$ (0.147 g, 1 mmol) were mixed in deionized water (10 mL) and mechanically stirred for two hours. Hdmpz (0.184 g, 2 mmol) was then added to the resulting solution and stirred for another hour (Scheme 1). Then, the reaction mixture was kept undisturbed in cool conditions (below 4 $^\circ\text{C}$) for crystallization, from which block-shaped blue single crystals were obtained after few days. The yield was: 0.548 g (84%). The analytically calculated for the $\text{C}_{20}\text{H}_{32}\text{Cl}_4\text{Cu}_2\text{N}_8$ were: C, 36.76%; H, 4.94%; and N, 17.15%. We found: C, 36.63%; H, 4.89%; and N, 17.10%. The FT-IR spectral data (KBr disc, cm^{-1}) were: 3345(s), 2924(w), 2841(w), 2726(w), 1573(m), 1466(w), 1267(m), 1160(w), 1045(s), 809(m), 702(w), 663(w), and 580(w).

2.3. Crystallographic Data Collection and Refinement

The crystallographic data collection of compounds 1 and 2 was carried out in a Bruker D8 Venture diffractometer with a Photon III 14 detector, using an Incoatec high brilliance μS DIAMOND Cu tube equipped with Incoatec Helios MX multilayer optics. The Bruker APEX4 program was used for the data reduction and cell refinements [54]. SADABS was

used for the scaling and absorption corrections [54]. Using Olex2 [55], the structures were solved with the XT structure solution program [56] using intrinsic phasing and refined with the XL refinement package [56] using least squares minimization. All non-hydrogen atoms were refined with anisotropic thermal parameters by full-matrix least-squares calculations on F^2 . Hydrogen atoms were inserted at calculated positions and refined as riders. The molecular structures and the packing diagrams were drawn using Diamond 3.2 [57]. The crystallographic results obtained for compounds **1** and **2** are summarized in Table 1.

Table 1. Crystallographic data and structure refinement details for compounds **1** and **2**.

Crystal Parameters	1	2
Empirical formula	C ₂₄ H ₁₈ ClCuN ₅ O ₄	C ₂₀ H ₃₂ Cl ₄ Cu ₂ N ₈
Formula weight	539.42	653.41
Temperature (K)	100.0	111.0
Wavelength (Å)	1.54178	1.54178
Crystal system	Triclinic	Monoclinic
Space group	$P\bar{1}$	$P2_1/c$
$a/\text{Å}$	9.6570(9)	8.6960(6)
$b/\text{Å}$	10.8732(10)	13.4486(9)
$c/\text{Å}$	11.9997(11)	11.8533(8)
α°	68.329(2)	90
β°	70.758(2)	106.117(2)
γ°	71.247(2)	90
Volume (Å ³)	1076.48(17)	1331.75(16)
Z	2	2
Calculated density (g/cm ³)	1.664	1.629
Absorption coefficient (mm ⁻¹)	2.965	5.872
F (000)	550.0	668.0
Crystal size (mm ³)	0.45 × 0.21 × 0.21	0.22 × 0.152 × 0.108
θ range for data collection (°)	8.166 to 136.698	10.59 to 133.154
Index ranges	−11 ≤ h ≤ 11, −13 ≤ k ≤ 13, −14 ≤ l ≤ 14	−10 ≤ h ≤ 8, −16 ≤ k ≤ 16, −14 ≤ l ≤ 14
Reflections collected	27,524	8827
Unique data (R_{int})	3909 (0.0523)	2336 (0.0359)
Refinement method	Full-matrix least-squares on F^2	Full-matrix least-squares on F^2
Data/restraints/parameters	3909/0/320	2528/0/205
Goodness-of-fit on F^2	1.162	1.188
Final R indices [$I > 2\sigma(I)$] $R1/wR2$	0.0412/0.1047	0.0435/0.1127
R indices (all data) $R1/wR2$	0.0413/0.1048	0.0439/0.1129
Largest diff. peak and hole (e.Å ⁻³)	0.65 and −0.71	1.35 and −0.32

CCDC163545 and 2163546 contain the supplementary crystallographic data for compounds **1** and **2**, respectively. These data can be obtained free of charge at <http://www.ccdc.cam.ac.uk> or from the Cambridge Crystallographic Data Centre (12Union Road, Cambridge CB2 1EZ, UK; fax: (+44) 1223-336-033; E-mail: deposit@ccdc.cam.ac.uk).

2.4. Theoretical Methods

The interaction energies of the compounds and supramolecular assemblies investigated in this work were computed at the RI-BP86-D3/def2-TZVP [58,59] level of theory using experimental geometries (only the H atoms were optimized) and the program Turbomole 7.2 [60]. We did not optimize the geometries because we were interested in estimating and characterizing the non-covalent forces as they stood in a solid state. Grimme's D3 dispersion [58] correction was used since it is convenient for the correct evaluation of non-covalent interactions, especially those involving π -systems, such as those investigated herein. The NCI plot [61] reduced density gradient (RGD) isosurfaces and QTAIM method [62] were combined in the same representation to characterize the non-covalent

interactions by means of the MULTIWFN program [63], and these were represented using VMD software [64].

3. Results

3.1. Synthesis and General Aspects

Compound **1** was prepared by the reaction between $\text{Cu}(\text{NO}_3)_2 \cdot 3\text{H}_2\text{O}$, CaCl_2 and phen (1:1:2) at room temperature in methanol medium. Similarly, compound **2** was synthesized by the reaction between $\text{Cu}(\text{NO}_3)_2 \cdot 3\text{H}_2\text{O}$, CaCl_2 and Hdmpz (1:1:2) at room temperature in de-ionized a water medium. Both the compounds are soluble in water and in common organic solvents. The compounds exhibited room temperature magnetic moment values of 1.76 and 1.74 BM, respectively, indicating the presence of one unpaired electron per Cu(II) center [65]. Crystallographic data collection at a lower temperature can improve the quality of the data sets, thereby resulting in more accurately solved crystal structures [66]. Simple synthetic procedures in aqueous media were followed for compounds **1** and **2**, and the crystal structures were redetermined at low temperatures and with different unit cell parameters (Tables S1 and S2) than the previously reported compounds [67–71]. Improved R and wR values for the compounds implied that there was improved crystallographic data collection for the compounds [72,73]. We also explored non-covalent $(\pi-\pi)_1/(\pi-\pi)_2/(\pi-\pi)_1$ and anion- $\pi/(\pi-\pi)$ /anion- π ternary assemblies in compound **1** and unconventional type I Cl...Cl interactions in compound **2** (vide infra). The supramolecular assemblies of the compounds were further established using various computational tools.

3.2. Crystal Structure Analysis

Figure 1 depicts the molecular structure of compound **1**. Selected bond lengths and bond angles are tabulated in Table 2. Compound **1** crystallized in the triclinic $P\bar{1}$ space group. The Cu(II) center in compound **1** was penta-coordinated with two bidentate phen moieties and one chloride moiety. The asymmetric unit of compound **1** contained one nitrate and one lattice water molecule. The coordination geometry around the Cu(II) center was square pyramidal, as evidenced by the trigonality index (τ) value of 0.25 [74,75]. The Cl atom (Cl1) occupied the apical position, whereas the equatorial positions were occupied by the four N atoms (N1, N1', N10, and N10') from the two phen moieties. The Cu–Cl and average Cu–N bond lengths were comparable to those of the already reported Cu(II) compounds [76,77].

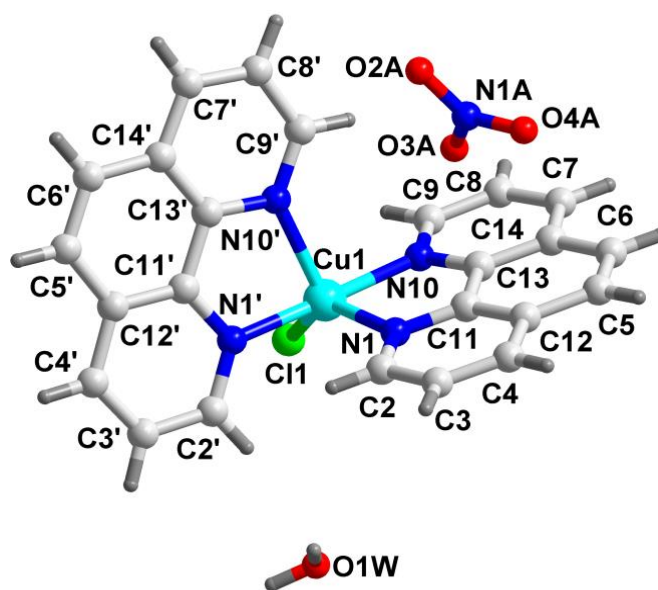


Figure 1. Molecular structure of $[\text{Cu}(\text{phen})_2\text{Cl}]\text{NO}_3 \cdot \text{H}_2\text{O}$ (**1**).

Table 2. Selected bond lengths (Å) and bond angles (°) of the Cu(II) centers in compounds **1** and **2**.

Compound 1			
Cu1–Cl1	2.2937(6)	N10–Cu1–N1	81.63(8)
Cu1–N1	2.0827(2)	N10–Cu1–N1#1	175.54(8)
Cu1–N10	1.987(2)	N10–Cu1–N10#1	96.83(8)
Cu1–N1#1	1.988(2)	N1#1–Cu1–Cl1	91.54(6)
Cu1–N10#1	2.137(2)	N1#1–Cu1–N1	95.25(8)
N1–Cu1–Cl1	139.47(6)	N1#1–Cu1–N10#1	80.79(8)
N1–Cu1–N10#1	104.12(7)	N10#1–Cu1–Cl1	116.41(5)
N10–Cu1–Cl1	92.90(6)		
Compound 2			
Cu1–Cl1#1	2.6558(1)	N1–Cu1–Cl1#1	100.44(9)
Cu1–Cl	2.3229(1)	Cl1–Cu1–Cl1#1	84.90(3)
Cu1–Cl2	2.2983(1)	N1–Cu1–Cl2	89.12(9)
Cu1–N1	2.013(3)	N1#–Cu1–Cl1#1	99.07(9)
Cu1–N1#	2.003(3)	N1#–Cu1–Cl1	89.41(9)
Cl2–Cu1–Cl1#1	98.65(3)	N1#–Cu1–Cl2	162.25(9)
Cl2–Cu1–Cl1	91.27(3)	N1#–Cu1–N1	88.56(1)
N1–Cu1–Cl1	174.53(9)	O5–Mn2–O5	86.70(6)

#1 2-X, 1-Y, 1-Z.

The lattice nitrate moieties and the complex cationic moieties of compound **1** were involved in the formation of the anion– π/π – π/π –anion assembly along the crystallographic ac plane (Figure 2a). The O3A atom of the lattice nitrate was involved in the anion– π interactions with the pyridyl ring of the coordinated phen, having a O3A...Cg distance of 3.56 Å, while the corresponding angle between the O3A–Cg plane of the ring was found to be 98.4° [78–80]. Aromatic π -stacking interactions were observed between the aromatic rings of the coordinated phen, having centroid–centroid separations of 3.53 and 3.87 Å, respectively. A C–H...Cl hydrogen-bonding interaction was observed between the coordinated Cl atom (Cl1) and the –CH moiety of the phen, having a C5–H5...Cl1 distance of 2.92 Å. The O3A atom of the lattice nitrate anion was also involved in the C–H...O hydrogen-bonding interactions, having a C9–H9...O3A distance of 2.80 Å. This anion– π/π – π/π –anion assembly observed in the crystal structure of compound **1** was further studied theoretically (vide infra). These anion– π/π – π/π –anion assemblies, along with lattice water molecule of compound **1**, were involved in the formation of the layered assembly along the crystallographic ac plane, which was stabilized by the C–H...O, C–H...Cl, O–H...Cl, and O–H...O hydrogen-bonding and the non-covalent C–H... π , π – π interactions (Figure 2b). The lattice nitrate and water molecule were interconnected via the O–H...O hydrogen-bonding interactions, having a O1W–H1WA...O2A distance of 1.94 Å. Similarly, the O4A atom of the lattice nitrate was involved in the C–H...O hydrogen-bonding interaction, having a C4–H4...O4A distance of 2.44 Å. The C–H...Cl hydrogen-bonding interactions were observed between the coordinated Cl atom (Cl1) and the –CH moiety of the phen, having a C6–H6...Cl1 distance of 2.98 Å. An O–H...Cl hydrogen-bonding interaction was observed between the coordinated Cl1 atom and the O1W lattice water molecule, having a O1W–H1WB...Cl1 distance of 2.33 Å. The –C3H3 moiety of the phen was involved in the C–H... π interaction, having C3...Cg and H3...Cg separation distances of 3.83 and 3.12 Å, respectively (Cg was the ring centroid defined by the atoms C5, C6, and C11–C14). Aromatic π -stacking interactions were observed between the phenyl moieties of the coordinated phen, having centroid–centroid separations of 3.62 and 3.61 Å, respectively.

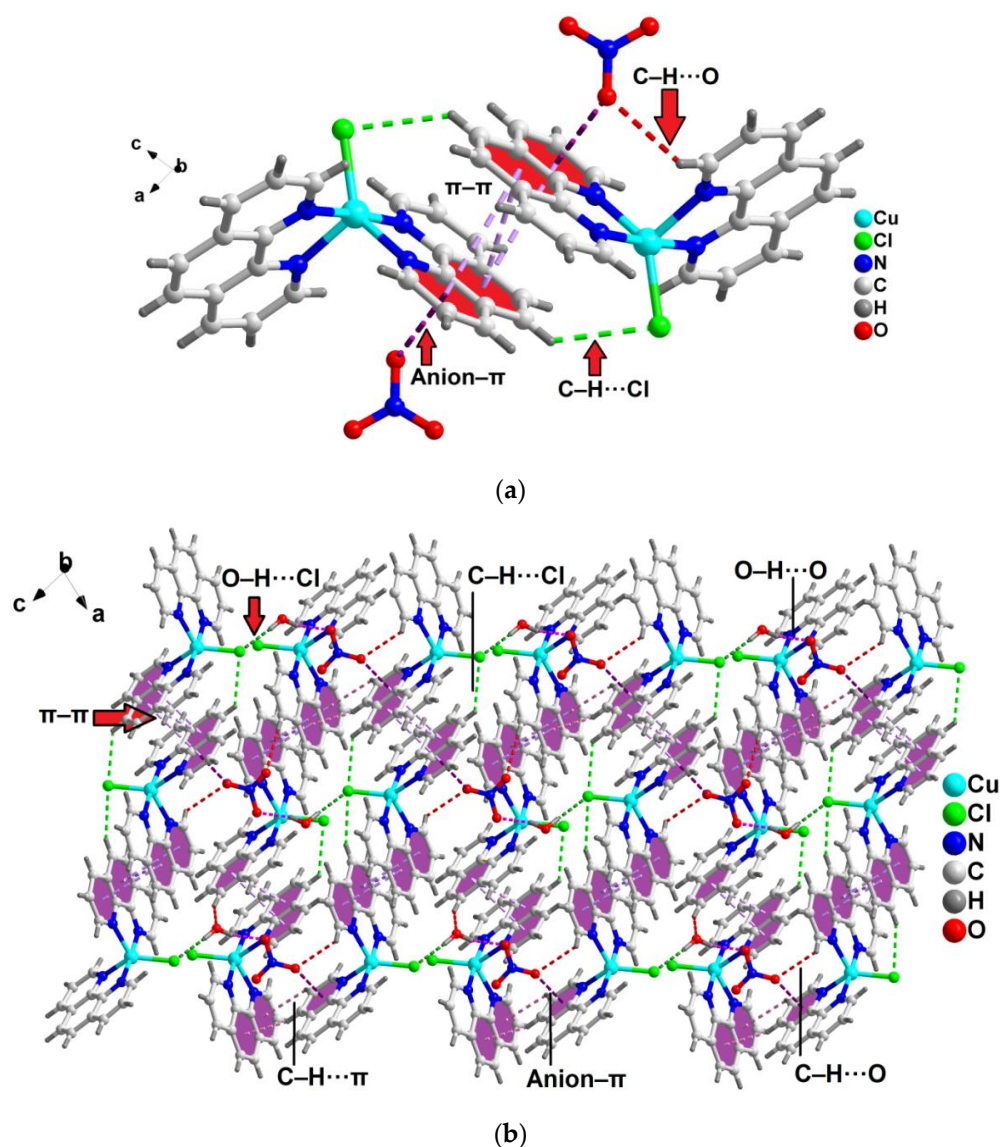


Figure 2. (a) Formation of the anion- π / π - π / π -anion assemblies in compound 1 involving the uncoordinated nitrate anions. (b) Layered assembly of compound 1 along the crystallographic ac plane aided by the anion- π / π - π / π -anion assemblies.

As shown in Figure S1, a 1D chain of compound 1 was formed via the C-H...Cl and π -stacking interactions. Cl1 and the -CH moieties of the coordinated phen were involved in the C-H...Cl hydrogen-bonding interactions, having C6'-H6'...Cl1 and C5'-H5'...Cl1 distances of 2.98 and 2.92 Å, respectively. Moreover, aromatic π -stacking interactions were observed between the neighboring phen moieties, having centroid-centroid separations of 3.61, 3.62, 3.87, 3.96, 3.46 and 3.53 Å, respectively.

The layered architecture of compound 1 was stabilized by the non-covalent C-H... π interactions (Figure S2). C-H... π interactions were observed between the -C4H4 moiety of the phen with the π -electron of the neighboring phen. The distance from the carbon atom (C4) to the π -electron of the phen was found to be 3.45 Å, whereas the distance from the hydrogen atom (H4) to the π -electron of the phen was found to be 2.53 Å. Moreover, the corresponding C-H... π angle was 120.4°, which indicated the significance of the interaction [81].

Figure 3 represents the molecular structure of compound 2. Selected bond lengths and bond angles are tabulated in Table 2. Compound 2 crystallized in the monoclinic $P2_1/c$ space group. Compound 2 was a dimeric Cu(II) compound-bridged by two Cl ions.

The coordination geometry around the Cu(II) centers were penta-coordinated with two pyrazole nitrogen atoms (N1 and N1') of two Hdmpz moieties, two bridging Cl ions (Cl1) and one monodentate Cl atom (Cl2). Compound 2 possessed a crystallographic inversion center of symmetry which was present at the center of the compound. The coordination geometries around the Cu(II) centers in compound 2 were distorted square pyramidal, as evidenced by the value of trigonality index (0.12), which was consistent with the square pyramidal geometry. The Cl atom (Cl2) was present at the axial site, whereas the equatorial sites were occupied by two nitrogen atoms (N1, N1') and two bridging Cl atoms (Cl1). The average Cu–Cl and Cu–N bond lengths were in good agreement with the previously reported similar compounds [82].

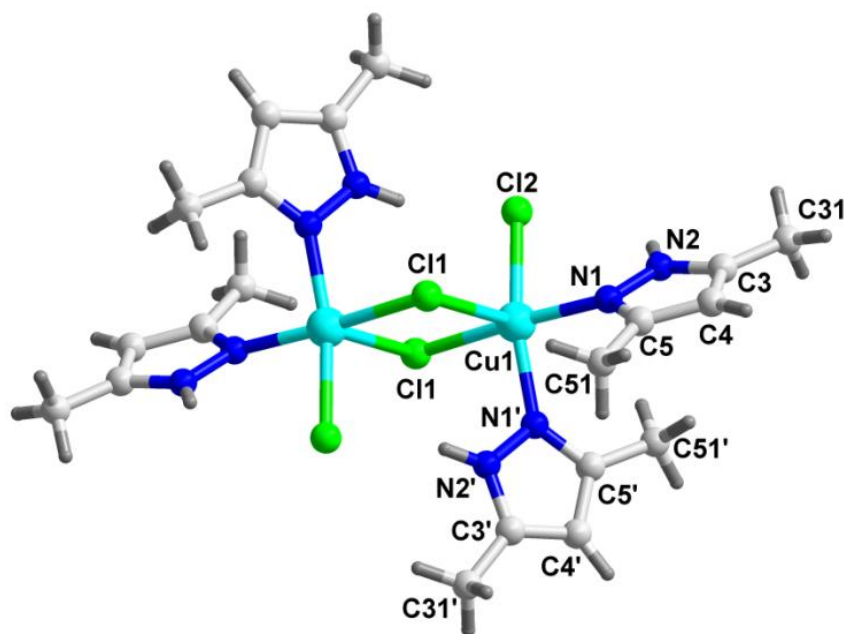


Figure 3. Molecular structure of $[\text{Cu}_2(\mu\text{-Cl}_2)\text{Cl}_2(\text{Hdmpz})_4]$ (compound 2).

As shown in Figure 4, the adjacent dinuclear units of compound 2 were interconnected via the N–H \cdots Cl and C–H \cdots Cl hydrogen-bonding, and non-covalent C–H \cdots C and unconventional Cl \cdots Cl contacts formed the 1D supramolecular chain along the crystallographic a-axis. N–H \cdots Cl contacts were observed, involving the coordinated Cl atom (Cl2) and the –NH (N2H2) moiety of the Hdmpz, having N–H \cdots Cl bond distances of 2.68 and 2.32 Å, respectively. Similarly, N–H \cdots Cl and C–H \cdots Cl interactions were also observed, having N2–H2 \cdots Cl1 and C31–H31C \cdots Cl2 distances of 2.99 and 3.02 Å, respectively. Non-covalent C–H \cdots C interactions [83] were involved in the stabilization of the 1D chain of compound 2 (Table S3). Moreover, unconventional Cl \cdots Cl interactions were also observed between the Cl atoms of the neighboring monomeric units, having Cl \cdots Cl separation distances of 3.58 Å. The Cl \cdots Cl interactions observed in the 1D supramolecular chain of compound 2 could be considered type I, with the corresponding angles $\theta_1 = \theta_2 = 91.5^\circ$. The type I Cl \cdots Cl interactions were explored in a Mn(II) coordination polymer, namely, $[\text{Mn}(\text{tcpa})_2(\text{bipy})]_n$ (where Htcpa and bipy represent 3,5,6-trichloropyridine-2-oxyacetic acid and 2,2'-bipyridine, respectively) [84]. The unconventional Cl \cdots Cl interactions (type I) were further established using the NCI plot computational tool (vide infra).

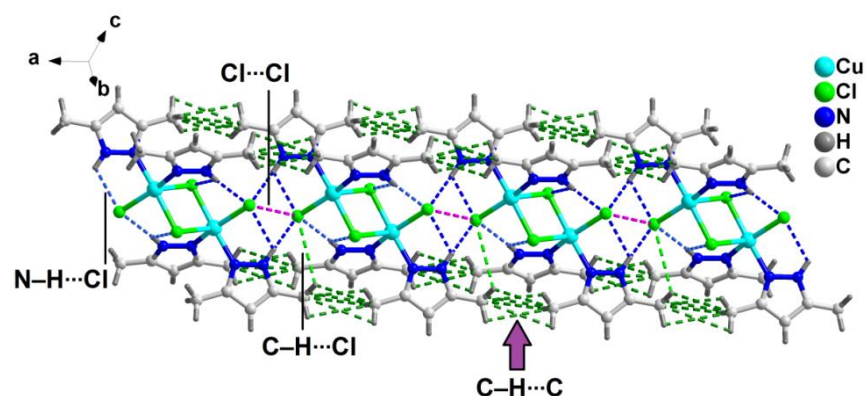


Figure 4. The 1D supramolecular chain of compound **2** assisted via the N-H...Cl, C-H...Cl hydrogen-bonding and the non-covalent C-H...C and unconventional Cl...Cl interactions.

Figure S3 represents the layered assembly of compound **2** along the crystallographic *ac* plane, as assisted by the non-covalent C-H...C interactions. The methyl groups of the Hdmpz moieties of the neighboring monomeric units were involved in the non-covalent C-H...C interactions (Table S3).

The neighboring monomeric units of compound **2** were also interconnected via the intermolecular C-H...Cl hydrogen-bonding and non-covalent C-H...C interactions to form a layered assembly along the crystallographic *ab* plane (Figure 5). The coordinated Cl (Cl2) atom was involved in the C-H...Cl hydrogen-bonding interactions with the -CH moiety of the Hdmpz, having a C51-H51B...Cl2 distance of 2.90 Å (Table 3). Moreover, the Cl1 atom was also involved in the C-H...Cl hydrogen-bonding interactions with the -CH moiety of the Hdmpz, having C31-H31E...Cl1 and C31-H31B...Cl1 distances of 2.99 and 2.89 Å, respectively. Furthermore, non-covalent C-H...C contacts were also observed in the layered assembly of compound **2** (Table S3).

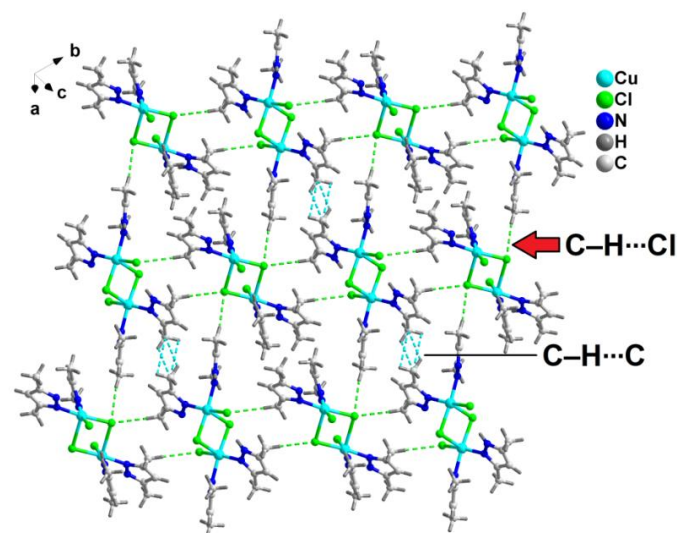


Figure 5. Layered assembly of compound **2** along the crystallographic *ab* plane, as assisted by the C-H...Cl hydrogen-bonding and non-covalent C-H...C interactions.

Table 3. Selected hydrogen bond distances (Å) and angles (°) for compounds **1** and **2**.

D–H···A	d(D–H)	d(D···A)	d(H···A)	<(DHA)
1				
C6'–H6'···Cl1	0.94	3.873(2)	2.98	156.7
C5'–H5'···Cl1	0.94	3.649(2)	2.92	133.7
C9–H9···O3A	0.94	3.215(2)	2.80	107.4
C4–H4···O4A	0.94	3.345(2)	2.44	157.5
O1W–H1WA···O2A	0.87	2.792(2)	1.94	164.3
O1W–H1WB···Cl1	0.87	3.203(3)	2.33	174.4
2				
N2–H2···Cl2	0.87	3.114(2)	2.68	111.3
N2–H2···Cl2	0.87	3.180(2)	2.32	164.9
N2–H2···Cl1	0.87	3.517(2)	3.00	119.4
C51–H51B···Cl1	0.97	3.820(2)	2.89	157.2
C31–H31E···Cl1	0.97	3.895(2)	3.00	151.8
C31–H31B···Cl1	0.97	3.859(2)	2.88	171.3

3.3. Spectral Studies

3.3.1. FT-IR Spectroscopy

The FT-IR spectral analyses of the compounds were completed in detail (see ESI; Figure S4). The absorption bands due to coordinated phen and Hdmpz moieties were obtained at the expected positions [85–89]. The presence of uncoordinated water and nitrate anions in the compounds could also be corroborated by their respective peaks [90,91].

3.3.2. Electronic Spectroscopy

Figures S5 and S6 depict the solid and aqueous phase electronic spectra of compounds **1** and **2**, respectively. The electronic spectra of the compounds suggested the presence of Cu(II) centers in the compounds [92]. The similar absorption bands in both the phases indicated that the compounds did not undergo any distortion in the aqueous phase [93–95].

3.4. Thermogravimetric Analysis

We recorded the thermogravimetric curves of compounds **1** and **2** in the temperature range of 25–800 °C under an N₂ atmosphere at a heating rate of 10 °C/min (Figure S7). For compound **1**, in the temperature range of 50–160 °C, the compound underwent a loss of water molecules of crystallization (obs. = 3.92%, calcd. = 3.39%) [96,97]. In the temperature range of 161–375 °C, the lattice nitrate and one phen moiety underwent decomposition, with a weight loss of 44.53% (calcd. = 44.52%) [98–100]. In the 376–790 °C range, Cl and half of the phen moiety underwent decomposition, with a 25.34% weight loss (calcd. = 23.68%) [97,99,100]. Beyond the temperature, the compounds decomposed in an unidentified manner. Compound **2** decomposed in a single step in the range of 51–370 °C, with the loss of four Cl and four Hdmpz moieties (obs. = 78.24%, calcd. = 79.34%) [96,101]. Compound **2** was likely to degrade to CuO at temperatures above 500 °C (Figure S8) [102].

3.5. Theoretical Study

The theoretical study was focused on the non-covalent interactions present in the compounds, particularly the anion- π / π - π / π -anion assemblies in compound **1** and the H bonds and Cl···Cl interactions in compound **2**. First, we computed the MEP surfaces of compounds **1** and **2** to investigate the most electrophilic and nucleophilic parts of the molecules. The MEP surfaces are represented in Figure 6, which discloses that the MEP minimum was located at the nitrate anion, as expected (−59 kcal/mol), followed by the chlorido ligand (−37 kcal/mol). The MEP maximum was located at the aromatic H atoms of the coordinated phen (25 kcal/mol); therefore, the formation of the H bonds between the aromatic protons and the counter ions (nitrate and chloride) were the most electrostatically favored contacts. Interestingly, the MEP values were small and positive

over the aromatic rings of the phen ligand (ranging from 3 to 6 kcal/mol). Such small MEP values facilitated the formation of the π -stacking interactions since the electrostatic repulsion was small and compensated by other attractive forces such as dispersion and polarization. It is interesting to highlight that the MEP value over the five-membered chelate ring was negative (-5 kcal/mol), thus favoring the formation of the antiparallel π -stacking interactions since the negative chelate ring was approximate to the positive central ring of the phen, as observed in compound **1**. Moreover, the antiparallel arrangement of the dipoles significantly increased the binding energy, as we previously demonstrated [103]. The MEP of compound **2** showed that the MEP maximum was located at one of the NH groups (37 kcal/mol) (the one that did not forming an intramolecular N-H \cdots Cl bond). The MEP was also large and positive at the H atoms of the CH₃ groups (~ 18 kcal/mol). The MEP minimum was located at the coordinated chlorido ligands (-48 kcal/mol); therefore, the most-favored interaction corresponded to the N-H \cdots Cl bonds, as observed in the solid state of compound **2**.

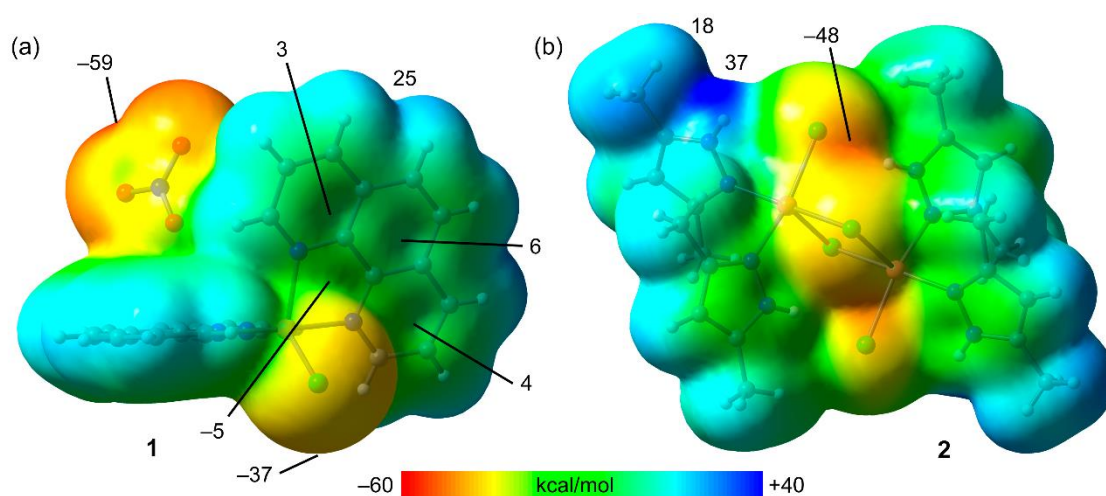


Figure 6. MEP surfaces of compounds **1** (a) and **2** (b) at the RI-BP86-D3/def2-TZVP level of theory. The isovalue was 0.001 a.u., and the energies at selected points are indicated in kcal/mol.

Figure 7 shows the anion- π / π - π /anion- π assembly observed in compound **1**, where two nitrate anions established an anion- π interaction with a π -stacked dimer, with a large overlap of the π -systems of the phen rings. The anion- π interaction likely reinforced the π -stacking by reducing the electrostatic repulsion between the π -acidic phen rings, i.e., the phen rings became electron-deficient upon coordination with the Cu(II) metal center. Such an effect was compensated by the anion- π interaction at the opposite side of the ring, as previously demonstrated in the literature [104,105]. A model of the anion- π / π - π /anion- π assembly is given in along with the interaction energy (computed as the π -stacked dimer) of $\Delta E_1 = -23.6$ kcal/mol, confirming that the antiparallel π -stacking was very strong. The assembly was further strengthened by the formation of the C-H \cdots Cl interactions, which was in good agreement with the MEP surface analysis discussed above. In order to estimate the contribution of the C-H \cdots Cl bonds, we computed a mutated model where the chlorido ligands were replaced by hydrido ligands. Consequently, the H bonds were not formed, and the interaction energy of the mutated dimer was reduced to $\Delta E_2 = -19.1$ kcal/mol, which corresponded to the π -stacking interaction, and the difference (-4.5 kcal/mol) corresponded to the C-H \cdots Cl hydrogen bonding. Therefore, the π -stacking interaction was the dominant force in this assembly.

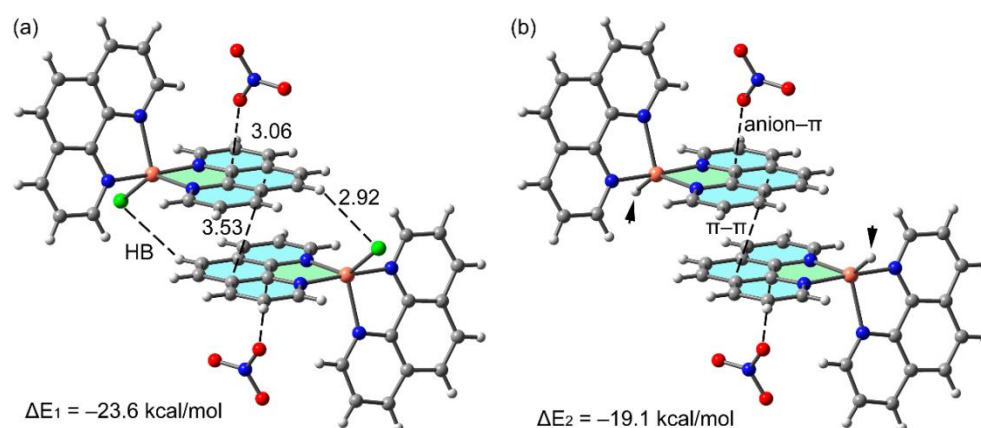


Figure 7. Complete (a) and mutated (b) theoretical models used to evaluate the π -stacking and C–H \cdots Cl H bonds in compound 1. The distances were measured in Å.

An H-bonded dimer extracted from the 1D supramolecular assembly of compound 2 was analyzed theoretically, as shown in Figure 8. We used red dashed lines to represent the intra-molecular N–H \cdots Cl bonds and black dashed lines to represent the intermolecular H bonds. Two different types of H bonds observed (N–H \cdots Cl and C–H \cdots Cl) were in good agreement with the MEP analysis shown in Figure 6b. The dimerization energy was quite large and negative ($\Delta E_3 = -24.7$ kcal/mol), thus evidencing the strong nature of these H bonds. In order to estimate the energy of the N–H \cdots Cl H-bonds, we used a mutated dimer, where one of the methyl groups of the organic ligand was replaced by H atoms (see the small arrows in Figure 8b).

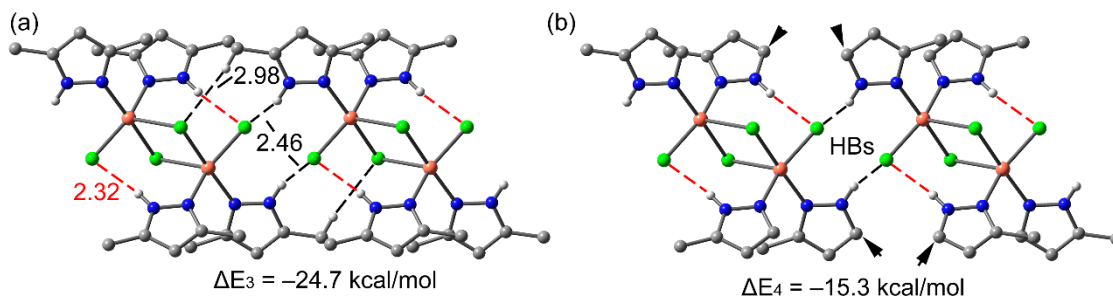


Figure 8. Complete (a) and mutated (b) theoretical models used to evaluate the N–H \cdots Cl and C–H \cdots Cl H bonds in compound 2. The distances were measured in Å. The H atoms have been omitted for clarity, apart from those that formed H bonds.

The interaction energy of the mutated dimer was reduced to $\Delta E_4 = -15.3$ kcal/mol, corresponding to the strength of the N–H \cdots Cl bonds, and the difference (9.4 kcal/mol) could be attributed to the C–H \cdots Cl and the additional van der Waals interactions, as discussed below.

Finally, a combination of the QTAIM and NCI plot (RDG isosurfaces) methods was used to characterize the interactions in the assemblies of compounds 1 and 2. The anion– π interaction was characterized by a bond critical point (CP, represented by a red sphere) and a bond path (represented by orange lines) connecting one O atom of nitrate to one C atom of the coordinated phen. The anion was further connected to the adjacent phen ligand by a C–H \cdots O H bond. The π -stacking interaction was characterized by six bond CPs and bond paths interconnecting several atoms of phen. Finally, the QTAIM also confirmed the existence of the C–H \cdots Cl interactions, characterized by a bond CP and a bond path interconnecting the H and Cl atoms.

All these interactions were also revealed by the RDG isosurfaces. It is interesting to highlight that the NCI plot RDG isosurface that characterized the antiparallel π -stacking

interactions involved the phen moieties (vide supra). For compound **2**, the distribution of the critical points showed that each H bond was characterized by a corresponding bond CP, bond path and green isosurface. Remarkably, the NCI plot analysis also evidenced a green isosurface between the Cl atoms, thus confirming the existence of a Cl...Cl contact and suggesting its weak attractive nature. Moreover, there were also several green RDG isosurfaces located between the methyl groups and the ligands, disclosing the existence of van der Waals interactions and explaining the large reduction in the interaction energy of compound **2** when the mutated dimer was used (see Figure 9). The density, Laplacian of density and energy densities at the bond CPs are given in Table 4. It could be observed that in all cases, the values of ρ were less than 0.01 a.u., and $Gr > |Vr|$, as is typical in closed shell non-covalent interactions.

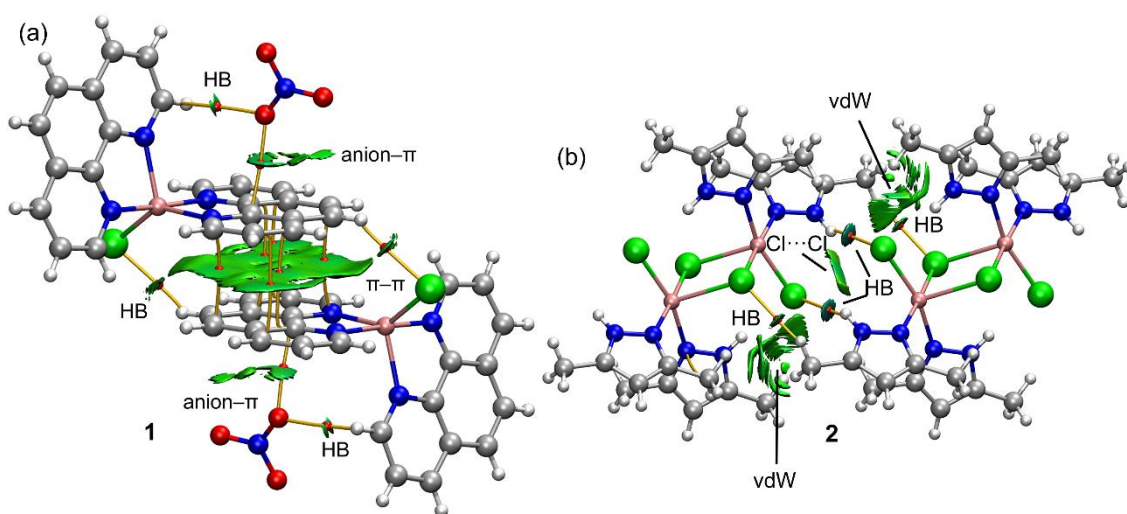


Figure 9. Combined QTAIM (bond CPs shown in red and bond paths shown as orange lines) and RDG isosurface analyses of the assemblies of compounds **1** (a) and **2** (b).

Table 4. QTAIM parameters at the bond CPs depicted in Figure 9. The density (ρ), Lagrangian kinetic energy density (Gr), potential energy density (Vr), total energy density (Hr) and Laplacian ($\nabla^2\rho$) are given in a.u.

Interaction	ρ	Gr	Vr	Hr	$\nabla^2\rho$
Dimer compound 1 (Figure 9a)					
CH...Cl	0.00695	0.00432	-0.00324	0.00108	0.02160
π ... π (N...C)	0.00526	0.00335	-0.00238	0.00098	0.01732
π ... π (C...C)	0.00625	0.00359	-0.00274	0.00085	0.01772
π ... π (C...C)	0.00541	0.00321	-0.00232	0.00089	0.01638
anion... π	0.00852	0.00634	-0.00477	0.00157	0.03162
CH...O (nitrate)	0.00615	0.00431	-0.00305	0.00125	0.02222
Dimer compound 2 (Figure 9b)					
CH...Cl	0.00593	0.00352	-0.00264	0.00089	0.01764
NH...Cl	0.01441	0.01014	-0.00768	0.00246	0.05041

4. Conclusions

Two coordination compounds of Cu(II) involving N-donor ligands (phen and Hdmpz) were synthesized and characterized using elemental analysis, TGA, spectroscopic (FT-IR and electronic) techniques and single crystal XRD. The lattice nitrate anion and the coordinated phen moieties of compound **1** were involved in unusual anion- π / $(\pi$ - $\pi)$ /anion- π assemblies which stabilized its crystal structure. The crystal structure analysis of compound **2** revealed the presence of unusual Cl...Cl contacts involving the coordinated Cl

moieties. Moreover, DFT calculations were performed to evaluate the strengths of the antiparallel π -stacking interactions, along with anion- π contacts, in compound **1**, evidencing the role of cooperative anion- π / $(\pi-\pi)$ /anion- π assemblies towards the stabilization of the compound. Similarly, in compound **2**, the H-bonding contacts were found to be the structure-guiding non-covalent forces, thereby stabilizing its crystal structure. These interactions were further characterized using the MEP surface, NCI plot and QTAIM computational tools.

Supplementary Materials: The following supporting information can be downloaded at: <https://www.mdpi.com/article/10.3390/cryst13030517/s1>, Figure S1: 1D supramolecular chain of compound **1** assisted by C-H \cdots Cl and π -stacking interactions; Figure S2: Layered assembly of compound **1** along the crystallographic ac plane; Figure S3: Layered assembly of compound **2** assisted by non-covalent C-H \cdots C interactions; Figure S4: FTIR spectra of compounds **1** and **2**; Figure S5: (a) UV-Vis-NIR spectrum of **2** (b) UV-Vis spectrum of **2** in water; Figure S6: (a) UV-Vis-NIR spectrum of **3** (b) UV-Vis spectrum of **3**; Figure S7: TGA curves of compounds **1** and **2**; Figure S8: Decomposition of various ligands in various steps of compounds **1–2** in TGA analysis, Table S1: Comparison of crystal parameters of compound **1** with the already reported compounds; Table S2: Comparison of crystal parameters of compound **2** with the already reported compound; Table S3: Selected parameters for C-H \cdots C interactions in compound **2**. References [92–95] are cited in the supplementary materials.

Author Contributions: Conceptualization, A.F. and M.K.B.; methodology, A.F. and M.K.B.; software, A.F. and R.M.G.; formal analysis, A.F.; investigation, P.S. and R.M.G.; data curation, M.B.-O.; writing—original draft preparation, P.S. and M.K.B.; writing—review and editing, M.K.B.; visualization, A.F.; supervision, M.K.B.; project administration, A.F. and M.K.B.; funding acquisition, A.F. and M.K.B. All authors have read and agreed to the published version of the manuscript.

Funding: Financial support was provided by ASTEC, DST, Govt. of Assam (grant number ASTEC/S&T/192(177)/2020-2021/43) and the Gobierno de Espana, MICIU/AEI (project number PID2020-115637GB-I00), all of whom are gratefully acknowledged. The authors thank IIT-Guwahati for the TG data.

Data Availability Statement: Not applicable.

Conflicts of Interest: The authors declare no conflict of interest. The funders had no role in the design of the study; in the collection, analyses, or interpretation of data; in the writing of the manuscript; or in the decision to publish the results.

References

1. Li, X.; Kang, Q.; Liu, L.; Ma, J.; Dong, W. Trinuclear Co(II) and mononuclear Ni(II) salamo-type bisoxime coordination compounds. *Crystals* **2018**, *8*, 43. [[CrossRef](#)]
2. Gu, J.; Wen, M.; Cai, Y.; Shi, Z.; Nesterov, D.S.; Kirillova, M.V.; Kirillov, A.M. Cobalt(II) coordination polymers assembled from unexplored pyridine-carboxylic acids: Structural diversity and catalytic oxidation of alcohols. *Inorg. Chem.* **2019**, *58*, 5875–5885. [[CrossRef](#)] [[PubMed](#)]
3. Tang, L.; Tang, L.; Wang, D.; Deng, H.; Chen, K. Metal and ligand effects on the stability and electronic properties of crystalline two-dimensional metal-benzenehexathiolate coordination compounds. *J. Phys. Condens. Matter* **2018**, *30*, 465301–465306. [[CrossRef](#)] [[PubMed](#)]
4. Abdel-Rahman, L.H.; Abdelhamid, A.A.; Abu-Dief, A.M.; Shehata, M.R.; Bakheeta, M.A. Facile synthesis, X-Ray structure of new multi-substituted aryl imidazole ligand, biological screening and DNA binding of its Cr(III), Fe(III) and Cu(II) coordination compounds as potential antibiotic and anticancer drugs. *J. Mol. Struct.* **2020**, *1200*, 127034–127045. [[CrossRef](#)]
5. Adam, R.; Mon, M.; Greco, R.; Kalinke, L.H.G.; Vidal-Moya, A.; Fernandez, A.; Winpenny, R.E.P.; Domenech-Carbo, A.; Leyva-Perez, A.; Armentano, D.; et al. Self-assembly of catalytically active supramolecular coordination compounds within metal-organic frameworks. *J. Am. Chem. Soc.* **2019**, *141*, 10350–10360. [[CrossRef](#)] [[PubMed](#)]
6. Gu, J.; Cai, Y.; Liang, X.; Wu, J.; Shi, Z.; Kirillov, A.M. Bringing 5-(3,4-dicarboxylphenyl)picolinic acid to crystal engineering research: Hydrothermal assembly, structural features and photocatalytic activity of Mn, Ni, Cu, and Zn coordination polymers. *CrystEngComm* **2018**, *20*, 906–916. [[CrossRef](#)]
7. Aakeroy, C.B.; Champness, N.R.; Janiak, C. Recent advances in crystal engineering. *CrystEngComm* **2010**, *12*, 22–43. [[CrossRef](#)]
8. Schiebi, J.; Schulmeister, J.; Doppiu, A.; Worner, E.; Rudolph, M.; Karch, R.; Hashmi, A.S.K. An industrial perspective on counter anions in gold catalysis: On alternative counter anions. *Adv. Synth. Catal.* **2018**, *360*, 3949–3954.

9. Khavasi, H.R.; Sadegh, B.M.M. Temperature-dependent supramolecular motif in coordination compounds. *Inorg. Chem.* **2010**, *49*, 5356–5358. [[CrossRef](#)]
10. Bi, W.Y.; Lv, X.Q.; Chai, W.L.; Jin, W.J.; Song, J.R.; Wong, W.K. Synthesis, structure and near-infrared (NIR) luminescence of three solvent-induced pseudo-polymorphic complexes from a bimetallic Zn–Nd Schiff-base molecular unit. *Inorg. Chem. Commun.* **2008**, *11*, 1316–1319. [[CrossRef](#)]
11. Bhattacharyya, M.K.; Saha, U.; Dutta, D.; Das, A.; Verma, A.K.; Frontera, A. Solvent-driven structural topology involving energetically significant intra- and intermolecular chelate ring contacts and anticancer activities of Cu(II) phenanthroline complexes involving benzoates: Experimental and theoretical studies. *RSC Adv.* **2019**, *9*, 16339–16356. [[CrossRef](#)]
12. Scheiner, S. *Non-Covalent Forces*; Springer: Dordrecht, The Netherlands, 2015.
13. Maharramov, A.M.; Mahmudov, M.K.; Kopylovich, M.N.; Pombeiro, A.J.L. (Eds.) *Non-Covalent Interactions in the Synthesis and Design of New Compounds*; John Wiley & Sons, Inc.: Hoboken, NJ, USA, 2016.
14. Desiraju, G.R. Chemistry beyond the molecule. *Nature* **2001**, *412*, 397–400. [[CrossRef](#)]
15. Mahmudov, K.T.; Kopylovich, M.N.; Silva, M.F.C.G.; Pombeiro, A.J.L. Non-covalent interactions in the synthesis of coordination compounds: Recent advances. *Coord. Chem. Rev.* **2017**, *345*, 54–72. [[CrossRef](#)]
16. Mahmudov, K.T.; Kopylovich, M.N.; Silva, M.F.C.G.; Pombeiro, A.J.L. Chalcogen bonding in synthesis, catalysis and design of materials. *Dalton Trans.* **2017**, *46*, 10121–10138. [[CrossRef](#)]
17. Sadhukhan, A.; Brandão, P.; Saha, S.; Mal, D.; Sepay, N. Insight into non-covalent interactions in 1D Gd-based coordination polymer for solid-state self-assembly through a new supramolecular synthon. *J. Mol. Struct.* **2023**, *1272*, 134204. [[CrossRef](#)]
18. Uslu, A.; Yeşilot, S. Recent advances in the supramolecular assembly of cyclophosphazene derivatives. *Dalton Trans.* **2021**, *50*, 2324–2341. [[CrossRef](#)]
19. Novikov, A.S. Non-Covalent Interactions in Organic, Organometallic, and Inorganic Supramolecular Systems Relevant for Medicine, Materials Science, and Catalysis. *Crystals* **2022**, *12*, 246. [[CrossRef](#)]
20. Weinhold, F.; Klein, R.A. What is a hydrogen bond? Mutually consistent theoretical and experimental criteria for characterizing H-bonding interactions. *Mol. Phys.* **2010**, *110*, 565–579. [[CrossRef](#)]
21. Mundlapati, V.R.; Sahoo, D.K.; Bhaumik, S.; Jena, S.; Chandrakar, A.; Biswal, H.S. Non-covalent carbon-bonding interactions in proteins. *Angew. Chem. Int. Ed.* **2018**, *57*, 16496–16500. [[CrossRef](#)]
22. Steed, J.W.; Atwood, J.L. *Supramolecular Chemistry*, 2nd ed.; John Wiley & Sons Ltd.: Chichester, UK, 2009.
23. Salonen, L.M.; Ellermann, M.; Diederich, F. Aromatic rings in chemical and biological recognition: Energetics and structures. *Angew. Chem. Int. Ed.* **2011**, *50*, 4808–4842. [[CrossRef](#)]
24. Neel, A.J.; Hilton, M.J.; Sigman, M.S.; Toste, F.D. Exploiting non-covalent π -interactions for catalyst design. *Nature* **2017**, *543*, 637–646. [[CrossRef](#)] [[PubMed](#)]
25. Mak, C.H. Unraveling base stacking driving forces in DNA. *J. Phys. Chem. B* **2016**, *120*, 6010–6020. [[CrossRef](#)]
26. Rather, I.A.; Wagay, S.A.; Ali, R. Emergence of anion- π interactions: The land of opportunity in supramolecular chemistry and beyond. *Coord. Chem. Rev.* **2020**, *415*, 213327–213396. [[CrossRef](#)]
27. Sharma, P.; Sarma, P.; Frontera, A.; Barcelo-Oliver, M.; Verma, A.K.; Sarma, B.; Barthakur, T.; Bhattacharyya, M.K. Energetically significant cooperative π -stacked ternary assemblies in Ni(II) phenanthroline compounds involving discrete water clusters: Anticancer activities and theoretical studies. *J. Mol. Struct.* **2021**, *1229*, 129486–129502. [[CrossRef](#)]
28. Nath, H.; Sharma, P.; Gomila, R.M.; Frontera, A.; Barceló-Oliver, M.; Verma, A.K.; Dutta, K.; Bhattacharyya, M.K. Unconventional enclathration of guest adipic acid and energetically significant antiparallel π -stacked ternary assemblies involving unusual region- π (chelate) contacts in phenanthroline-based Ni(II) and Cu(II) compounds: Antiproliferative evaluation and theoretical studies. *J. Mol. Struct.* **2021**, *1245*, 131038–131049.
29. Belkova, N.V.; Epstein, L.M.; Filippov, O.A.; Shubina, E.S. Hydrogen and dihydrogen bonds in the reactions of metal hydrides. *Chem. Rev.* **2016**, *116*, 8545–8587. [[CrossRef](#)]
30. Avdeeva, V.V.; Vologzhanina, A.V.; Malinina, E.A.; Kuznetsov, N.T. Dihydrogen bonds in salts of boron cluster anions $[B_nH_n]^{2-}$ with protonated heterocyclic organic bases. *Crystals* **2019**, *9*, 330. [[CrossRef](#)]
31. Kravchenko, E.A.; Gippius, A.A.; Kuznetsov, N.T. Non-covalent interactions in compounds based on perchlorinated boron cluster as monitored by ^{35}Cl NQR. *Russ. J. Inorg. Chem.* **2020**, *65*, 546–566. [[CrossRef](#)]
32. Juárez-Pérez, E.J.; Núñez, R.; Viñas, C.; Sillanpää, R.; Teixidor, F. The role of C–H \cdots H–B interactions in establishing rotamer configurations in metallabis(dicarbollide) systems. *Eur. J. Inorg. Chem.* **2010**, *21*, 2385–2392. [[CrossRef](#)]
33. Desiraju, G.R.; Ho, P.S.; Kloo, L.; Legon, A.C.; Marquardt, R.; Metrangolo, P.; Politzer, P.; Resnati, G.; Rissanen, K. Definition of the halogen bond. *Pure Appl. Chem.* **2013**, *85*, 1711–1713. [[CrossRef](#)]
34. Panini, P.; Boel, E.; Meervelt, L.V.; Mooter, G.V. Solvatomorphism in miconazole: The role of weak C–H \cdots Cl hydrogen bonds and C–Cl \cdots Cl–C Halogen interactions in similarities and differences in the crystal packing. *Cryst. Growth Des.* **2022**, *22*, 2703–2724. [[CrossRef](#)]
35. Cavallo, G.; Metrangolo, P.; Milani, R.; Pilati, T.; Priimagi, A.; Resnati, G.; Terraneo, G. The halogen bond. *Chem. Rev.* **2016**, *116*, 2478–2601. [[CrossRef](#)]
36. Wang, R.; Dols, T.S.; Lehmann, C.W.; Englert, U. The halogen bond made visible experimental charge density of a very short intermolecular Cl \cdots Cl donor-acceptor contact. *Chem. Commun.* **2012**, *48*, 6830–6832. [[CrossRef](#)]

37. Buifeld, D.; Engelage, E.; Mancheski, L.; Stoesser, J.; Huber, S.M. Crystal engineering with multipoint halogen bonding: Double two point donors and acceptors at work. *Chem. Eur. J.* **2020**, *26*, 1567–1575.
38. Hoque, M.N.; Das, G. Overview of the strategic approaches for the solid-state recognition of hydrated anions. *CrystEngComm* **2017**, *19*, 1343–1360. [[CrossRef](#)]
39. Aletti, A.B.; Blasco, S.; Aramballi, S.J.; Kruger, P.E.; Gunnlaugsson, T. Sulfate-templated 2D anion-layered supramolecular self-assemblies. *Chem* **2019**, *5*, 2617–2629. [[CrossRef](#)]
40. Deegan, C.; McCann, M.; Devereux, M.; Coyle, B.; Egan, D.A. *In vitro* cancer chemotherapeutic activity of 1,10-phenanthroline (phen), [Ag₂(phen)₃(mal)]·2H₂O, [Cu(phen)₂(mal)]·2H₂O and [Mn(phen)₂(mal)]·2H₂O (malH₂ = malonic acid) using human cancer cells. *Cancer Lett.* **2007**, *247*, 224–233. [[CrossRef](#)]
41. Prugovečki, B.; Vušak, D.; Ležaić, K.; Jurković, M. Ternary coordination compounds of copper with amino acids and 1,10-phenanthroline—structural insight and biological activity. *Acta Cryst.* **2021**, *A77*, 975–983. [[CrossRef](#)]
42. Vušak, D.; Ležaić, K.; Jurec, J.; Žilić, D.; Prugovečki, B. Solvent effects on the crystallization and structure of ternary copper(II) coordination compounds with l-threonine and 1,10-phenanthroline. *Heliyon* **2022**, *8*, 9556–9567. [[CrossRef](#)]
43. Avdeeva, V.V.; Malinina, E.A.; Zhizhin, K.Y.; Kuznetsov, N.T. Structural diversity of cationic copper(II) complexes with neutral nitrogen-containing organic ligands in compounds with boron cluster anions and their derivatives. *Russ. J. Inorg. Chem.* **2020**, *65*, 514–534. [[CrossRef](#)]
44. Bencini, A.; Lippolis, V. 1,10-Phenanthroline: A versatile building block for the construction of ligands for various purposes. *Coord. Chem. Rev.* **2010**, *254*, 2096–2180. [[CrossRef](#)]
45. Teixeira, F.J.; Flores, L.S.; Valverde, T.; Escobar, L.B.L.; Reis, M.S.; Corrêa, C.C. Synthesis and magnetic properties of two cobalt-coordination polymers containing 1,10-phenanthroline and alkyl dicarboxylates ligands. *J. Mol. Struct.* **2022**, *1261*, 132820. [[CrossRef](#)]
46. Romo, A.I.B.; Reis, M.P.; Nascimento, O.R.; Bernhardt, P.V.; Rodríguez-López, J.; Diógenes, I.C.N. Interplay of electronic and geometric structure on Cu phenanthroline, bipyridine and derivative complexes, synthesis, characterization, and reactivity towards oxygen. *Coord. Chem. Rev.* **2023**, *477*, 214943. [[CrossRef](#)]
47. Beheshti, A.; Mousavifard, E.S.; Noorzadeh, S.; Mayer, P.; Woźniak, K. Impact of cyanide co-ligand to convert crystal structure of pyrazole-based copper coordination compounds from a dinuclear to a polymeric structure and DFT calculations of [Cu₂(ttmp)X₂] (X = Cl and I). *Inorg. Chim. Acta* **2019**, *497*, 119082–119091. [[CrossRef](#)]
48. Direm, A.; Bali, B.E.; Sayin, K.; Abdelbaky, M.S.M.; Garcia-Granda, S. Experimental and *in silico* studies of dichloro-tetrakis(1H-pyrazole)-cobalt(II): Structural description, photoluminescent behavior and molecular docking. *J. Mol. Struct.* **2021**, *1235*, 130266–130280. [[CrossRef](#)]
49. Kreiger, D.I.; Mathivathanan, L.; Raptis, R.G. Coordination polymers based on pyrazole-4-carboxaldehyde-containing Cu₃N₆metallacycles as building units. *CrystEngComm* **2019**, *21*, 3047–3055. [[CrossRef](#)]
50. Mörtel, M.; Lindner, T.; Scheurer, A.; Heinemann, F.W.; Khusniyarov, M.M. Phenanthroline-based molecular switches for prospective chemical grafting: A synthetic strategy and its application to spin-crossover complexes. *Inorg. Chem.* **2020**, *59*, 2659–2666. [[CrossRef](#)]
51. Saleh, D.I.; Mahmoud, S.F.; Etaiw, S.E.H. Nanoscale supramolecular architectures assembly of copper cyanide, organotin, and 1,10-phenanthroline coordination polymers: Design and biological applications. *Appl. Organomet. Chem.* **2021**, *35*, 6247–6258. [[CrossRef](#)]
52. Champaka, G.; Senthilkumar, K.; David, E.; Shanmugan, S.; Palanisami, N. Monomeric zinc ferrocene carboxylate [Zn(FcCOO)(3,5-dmp)₂Cl] derived from 3,5-dimethylpyrazole: Structural, optical, electrochemical and antimicrobial studies. *J. Mol. Struct.* **2021**, *1228*, 129749–129758. [[CrossRef](#)]
53. Tayo, A.D.; Djoumbissie, A.; Golngar, D.; Fomuta, T.R.; Tagne, A.C.K.; Anguile, J.J.; Ngoune, J.N.; Eleuterio, A. Syntheses, characterization and DFT studies of two new homo-dinuclear zinc(II) complexes based on pyrazole and 3,5-dimethylpyrazole ligands. *J. Coord. Chem.* **2020**, *73*, 2055–2068. [[CrossRef](#)]
54. APEX3, SAINT, SADABS and XP, Bruker AXS Inc.: Madison, WI, USA, 2015.
55. Sheldrick, G.M. Crystal structure refinement with SHELXL. *Acta Crystallogr. Sect. A Found. Crystallogr.* **2008**, *64*, 112–122. [[CrossRef](#)]
56. Farrugia, L.J. WinGX and ORTEP for Windows: An update. *J. Appl. Crystallogr.* **1999**, *32*, 837–838. [[CrossRef](#)]
57. Brandenburg, K. *Diamond 3.1f*; Crystal Impact GbR: Bonn, Germany, 2008.
58. Grimme, S.; Antony, J.; Ehrlich, S.; Krieg, H. A consistent and accurate *ab initio* parametrization of density functional dispersion correction (DFT-D) for the 94 elements H–Pu. *J. Chem. Phys.* **2010**, *132*, 154104–154119. [[CrossRef](#)]
59. Weigend, F. Accurate Coulomb-fitting basis sets for H to Rn. *Phys. Chem. Chem. Phys.* **2006**, *8*, 1057–1065. [[CrossRef](#)]
60. Ahlrichs, R.; Bar, M.; Hacer, M.; Horn, H.; Kömel, C. Electronic structure calculations on workstation computers: The program system turbomole. *Chem. Phys. Lett.* **1989**, *162*, 165–169. [[CrossRef](#)]
61. Contreras-Garcia, J.; Johnson, E.R.; Keinan, S.; Chaudret, R.; Piquemal, J.P.; Beratan, D.N.; Yang, W. NCIPLOT: A program for plotting non-covalent interaction regions. *J. Chem. Theory Comput.* **2011**, *7*, 625–632. [[CrossRef](#)]
62. Bader, R.F.W. Atoms in molecules. *Chem. Rev.* **1991**, *91*, 893–928. [[CrossRef](#)]
63. Lu, T.; Chen, F. Multiwfn: A multifunctional wavefunction analyzer. *J. Comput. Chem.* **2012**, *33*, 580–592. [[CrossRef](#)]
64. Humphrey, J.W.; Dalke, A.; Schulten, K. VMD: Visual molecular dynamics. *J. Mol. Graph.* **1996**, *14*, 33–38. [[CrossRef](#)]

65. Al-Fakeh, M.S.; Allazzam, G.A.; Yarkandi, N.H. Ni(II), Cu(II), Mn(II) and Fe(II) metal complexes containing 1,3-Bis(diphenylphosphino)propane and pyridine derivative: Synthesis, characterization, and antimicrobial activity. *Int. J. Biomat.* **2021**, *44*, 4981367. [CrossRef]
66. Kottke, T.; Stalk, D. Crystal handling at low temperatures. *J. Appl. Cryst.* **1993**, *26*, 615–619. [CrossRef]
67. Chandrasekhar, V.; Kingsley, S.; Vij, A.; Lam, K.C.; Rheingold, A.L. Formation of a tetranuclear copper(II) cluster assembled by metal-assisted hydrolysis and desulfurization of bis(3,5-dimethylpyrazolyl)methylphosphinesulfide, MeP(S)(3,5-Me₂Pz)₂. *Inorg. Chem.* **2000**, *39*, 3238–3242. [CrossRef]
68. Gogoi, G.; Nath, J.K.; Hoque, N.; Biswas, S.; Gour, N.K.; Kalita, D.J.; Bora, S.R.; Bania, K.K. Single and multiple site Cu(II) catalysts for benzyl alcohol and catechol oxidation reactions. *Appl. Catal. A* **2022**, *644*, 118816–118832. [CrossRef]
69. Boys, D. Structure of Chlorobis(1, 10-phenanthroline)copper(II) Nitrate Monohydrate. *Acta Cryst.* **1988**, *C44*, 1539–1541.
70. Kumari, N.; Ward, B.D.; Kar, S.; Mishra, L. Reactivity of nitrilotriacetic acid with polypyridyl protected as well as naked copper(II) nitrate. *Polyhedron* **2012**, *33*, 425–434. [CrossRef]
71. Li, M. CCDC 726816; CSD Communication: Austin, TX, USA, 2020. [CrossRef]
72. Sheldrick, G.M. *A Short History of SHELX, SHELXTL Reference Manual*; Bruker-AXS, Inc.: Madison, WI, USA, 1997.
73. Wilson, A.J.C. Statistical bias in least-squares refinement. *Acta Cryst.* **1976**, *A32*, 994–996. [CrossRef]
74. Addison, A.W.; Rao, T.; Reedijk, J.; Rijn, J.V.; Verschoor, G. Synthesis, structure and spectroscopic properties of copper(II) compounds containing nitrogen–sulphur donor ligands; the crystal and molecular structure of aqua[1,7-bis(N-methylbenzimidazol-2'-yl)-2,6-dithiaheptane]copper(II) perchlorate. *Dalton Trans.* **1984**, *7*, 1349–1356. [CrossRef]
75. Sancheti, R.S.; Bendre, R.S.; Kumbhar, A.A. Cu(II), Ni(II), Zn(II) and Fe(III) complexes containing a N₂O₂ donor ligand: Synthesis, characterization, DNA cleavage studies and crystal structure of [Cu(HL)Cl]. *Polyhedron* **2012**, *31*, 12–18. [CrossRef]
76. Youngme, S.; Wannarit, N.; Pakawatchai, C.; Chaichit, N.; Somsook, E.; Turpeinen, U.; Mutikainen, I. Structural diversities and spectroscopic properties of bis and tris (1,10-phenanthroline) copper(II) complexes. *Polyhedron* **2007**, *26*, 1459–1468. [CrossRef]
77. Dutta, D.; Nath, H.; Frontera, A.; Bhattacharyya, M.K. A novel oxalato bridged supramolecular ternary complex of Cu(II) involving energetically significant π -hole interaction: Experimental and theoretical studies. *Inorg. Chim. Acta* **2019**, *487*, 354–361. [CrossRef]
78. Islam, S.M.N.; Dutta, D.; Sharma, P.; Verma, A.K.; Frontera, A.; Bhattacharyya, M.K. Supramolecular association involving antiparallel CO \cdots CO and anion– π contacts in Co(II) and Mn(II) complexes involving 2,5-pyridinedicarboxylate: Anticancer evaluation and theoretical studies. *Inorg. Chim. Acta* **2019**, *498*, 119108–119118. [CrossRef]
79. Garau, C.; Frontera, A.; Quinonero, D.; Russo, N.; Deya, P.M. RI-MP2 and MPWB1K study of π -anion– π' complexes: MPWB1K performance and some additivity aspects. *J. Chem. Theory Comput.* **2011**, *7*, 3012–3018. [CrossRef]
80. Sharma, P.; Sarma, P.; Frontera, A.; Hussain, S.; Verma, A.K.; Bhattacharyya, M.K. Energetically Significant Anti-parallel π -stacking and Unconventional Anion– π interactions in Phenanthroline based Ni(II) and Cu(II) Coordination Compounds: Antiproliferative Evaluation and Theoretical Studies. *Inorg. Chim. Acta* **2021**, *516*, 120082–120093. [CrossRef]
81. Gogoi, A.; Das, A.; Frontera, A.; Verma, A.K.; Bhattacharyya, M.K. Energetically significant unconventional π - π contacts involving fumarate in a novel coordination polymer of Zn(II): In-vitro anticancer evaluation and theoretical studies. *Inorg. Chim. Acta* **2019**, *493*, 1–13. [CrossRef]
82. Chkirate, K.; Fettach, S.; Karrouchi, K.; Sebbar, N.K.; Essassi, M.; Mague, J.T.; Radi, S.; Faouzi, A.; Adarsh, N.N.; Garcia, Y. Novel Co(II) and Cu(II) coordination complexes constructed from pyrazole-acetamide: Effect of hydrogen bonding on the self assembly process and antioxidant activity. *J. Inorg. Biochem.* **2019**, *191*, 21–28. [CrossRef]
83. Das, A.; Sharma, P.; Frontera, A.; Verma, A.K.; Barcelo-Oliver, M.; Hussain, S.; Bhattacharyya, M.K. Energetically significant nitrile \cdots nitrile and unconventional C–H \cdots π (nitrile) interactions in pyridine based Ni(II) and Zn(II) coordination compounds: Antiproliferative evaluation and theoretical studies. *J. Mol. Struct.* **2020**, *1223*, 129246–129259. [CrossRef]
84. Li, J.; Du, Z.; Pan, Q.; Zhang, L.; Liu, D. The first 3,5,6-trichloropyridine-2-oxyacetate bridged manganese coordination polymer with features of π \cdots π stacking and halogen \cdots halogen interactions: Synthesis, crystal analysis and magnetic properties. *Inorg. Chim. Acta* **2020**, *509*, 119677–119682. [CrossRef]
85. Nakamoto, K. *Infra-Red and Raman Spectra of Inorganic and Coordination Compounds*; John Wiley: New York, NY, USA, 1997.
86. Prashanthi, Y.; Kiranmai, K.; Subhashini, N.J.P. Synthesis, potentiometric and antimicrobial studies on metal complexes of isoxazole Schiff bases. *Spectrochim. Acta* **2008**, *70*, 30–35. [CrossRef]
87. Sharma, R.P.; Singh, A.; Brandao, P.; Felix, V.; Venugopalan, P. Role of non-covalent interactions in binding of non-coordinating anions: Syntheses, characterization and single crystal structure determination of cobalt(III) complexes with 2,2'-biimidazole and 1,10-phenanthroline ligands. *Inorg. Chem.* **2011**, *376*, 64–72. [CrossRef]
88. Dakovic, M.; Vinkovic, M.; Roca, S.; Popovic, Z.; Vickovic, I.; Vikić-Topić, D.; Lukac, J.; Dakovic, N.; Kusic, Z. Structural study of picolinamide complexes of Ni(II), Zn(II), Cd(II), and Hg(II) nitrates in solid state and solution. *J. Coord. Chem.* **2012**, *65*, 1017–1032. [CrossRef]
89. Direm, A.; Tursun, M.; Parlak, C.; Cherif, N.B. Trans-dichlorotetrakis (1H-pyrazole- κ N²) copper(II): Synthesis, crystal structure, hydrogen bonding graph-sets, vibrational and DFT studies. *J. Mol. Struct.* **2015**, *1093*, 208–218. [CrossRef]
90. Mahapatra, T.S.; Bauza, A.; Dutta, D.; Mishra, S.; Frontera, A.; Ray, D. Carboxylate coordination assisted aggregation for quasi-tetrahedral and partial-dicubane [Cu₄] coordination clusters. *ChemistrySelect* **2016**, *1*, 64–75. [CrossRef]

91. Wang, Y.; Lin, X.M.; Bai, F.Y.; Sun, L.X. Novel vanadium complexes with rigid carboxylate ligands: Synthesis, structure and catalytic bromine dynamics of phenol red. *J. Mol. Struct.* **2017**, *1149*, 379–386. [[CrossRef](#)]
92. Tandon, S.S.; Chen, L.; Thompson, L.K.; Bridson, J.N. Dinuclear copper(II) complexes of the tetradentatethiadiazole ligands BPMTD (2,5-bis((2-pyridylmethyl)thio)thiadiazole) and BPTD (2,5-bis(2-pyridylthio)thiadiazole). X-ray structures of $[\text{Cu}_2(\text{BPTD})(\mu^2\text{-Br})_2\text{Br}_2]$ and $[\text{Cu}(\text{BPMTD})\text{Cl}_2]_n$ and spectroscopic, electrochemical, and magnetic studies. *Inorg. Chem.* **1994**, *33*, 490–497.
93. Yenikaya, C.; Poyraz, M.; Sari, M.; Demirci, F.; Ilkimen, H.; Buyukgungor, O. Synthesis, characterization and biological evaluation of a novel Cu(II) complex with the mixed ligands 2,6-pyridinedicarboxylic acid and 2-aminopyridine. *Polyhedron* **2009**, *28*, 3526–3532. [[CrossRef](#)]
94. Bhattacharyya, M.K.; Saha, U.; Dutta, D.; Frontera, A.; Verma, A.K.; Sharma, P.; Das, A. Unconventional DNA-relevant π -stacked hydrogen bonded arrays involving supramolecular guest benzoate dimers and cooperative anion- π/π - π/π -anion contacts in coordination compounds of Co(II) and Zn(II) phenanthroline: Experimental and theoretical studies. *New J. Chem.* **2020**, *44*, 4504–4518. [[CrossRef](#)]
95. Kumar, S.; Sharma, R.P.; Venugopalan, P.; Aree, T.; Ferretti, V. Synthesis, spectroscopic characterization, single crystal X-ray analysis and DFT calculation of isomeric $\text{Cu}(\text{MR})_2(\beta/\gamma\text{-pic})_2$ complexes: First transition metal complexes of methyl red. *J. Mol. Struct.* **2018**, *1166*, 388–396. [[CrossRef](#)]
96. Demir, S.; Kantar, G.K.; Topcu, Y.; Li, Q. Solvothermal synthesis and characterization of coordination polymers of cobalt(II) and zinc(II) with succinic acid. *Transit. Met. Chem.* **2012**, *37*, 257–263. [[CrossRef](#)]
97. Yang, Q.; Chen, S.; Gao, S. Two Mn(II) chloride complexes containing guest molecules. *J. Therm. Anal. Calorim.* **2007**, *89*, 567–571. [[CrossRef](#)]
98. Carp, O.; Patron, L.; Diamandescu, L.; Reller, A. Thermal decomposition study of the coordination compound $[\text{Fe}(\text{urea})_6](\text{NO}_3)_3$. *Thermochim. Acta* **2002**, *390*, 169–177. [[CrossRef](#)]
99. Qi, Y.; Wang, Y.; Hu, C.; Cao, M.; Mao, L.; Wang, E. A new type of single-helix coordination polymer with mixed ligands $[\text{M}_2(\text{phen})_2(\text{e},\text{a}\text{-cis-1,4}\text{-chdc})(\text{H}_2\text{O})_2]_n$ (M = Co and Ni; phen = 1,10-phenanthroline; chdc = cyclohexanedicarboxylate). *Inorg. Chem.* **2003**, *42*, 8519–8523. [[CrossRef](#)]
100. Hwang, I.H.; Jo, Y.D.; Kim, H.Y.; Kang, J.; Noh, J.Y.; Hyun, M.Y.; Kim, C.; Kim, Y.; Kim, S.J. Novel Mn^{II} coordination compounds constructed from benzoate and various bipyridyl ligands: Magnetic property and catalytic activity. *Polyhedron* **2012**, *42*, 282–290. [[CrossRef](#)]
101. Takahashi, P.M.; Netto, A.V.G.; Mauro, A.E.; Frem, R.C.G. Thermal study of nickel(II) pyrazolyl complexes. *J. Therm. Anal. Calorim.* **2005**, *79*, 335–338. [[CrossRef](#)]
102. Sharma, R.P.; Saini, A.; Kumar, J.; Kumar, S.; Venugopalan, P.; Ferretti, V. Coordination complexes of copper(II) with herbicide-trichlorophenoxyacetate: Syntheses, characterization, single crystal X-ray structure and packing analyses of monomeric $[\text{Cu}(\gamma\text{-pic})_3(2,4,5\text{-trichlorophenoxyacetate})]\cdot\text{H}_2\text{O}$, $[\text{trans-Cu}(\text{en})_2(2,4,5\text{-trichlorophenoxyacetate})_2]\cdot 2\text{H}_2\text{O}$ and dimeric $[\text{Cu}_2(\text{H}_2\text{tea})_2(2,4,5\text{-trichlorophenoxyacetate})_2]\cdot 2(\text{H}_2\text{O})$. *Inorg. Chim. Acta* **2017**, *457*, 59–68.
103. Saha, U.; Dutta, D.; Nath, H.; Franconetti, A.; Frontera, A.; Bhattacharyya, M.K. Supramolecular association in Cu(II) coordination complexes involving energetically significant $\text{NO}\cdots\text{NO}$ π -hole interaction and cooperative π -stacked ternary assembly: Experimental and theoretical studies. *Inorg. Chim. Acta* **2019**, *488*, 159–169. [[CrossRef](#)]
104. Mitra, M.; Manna, P.; Seth, S.K.; Das, A.; Meredith, J.; Helliwell, M.; Bauza, A.; Choudhury, S.R.; Frontera, A.; Mukhopadhyay, S. Salt-bridge- π (sb- π) interactions at work: Associative interactions of sb- π , π - π and anion- π in Cu(II)-malonate-2-aminopyridine-hexafluoridophosphate ternary system. *CrystEngComm* **2013**, *15*, 686–696. [[CrossRef](#)]
105. Das, A.; Choudhury, S.R.; Estarellas, C.; Dey, B.; Frontera, A.; Hemming, J.; Helliwell, M.; Gamez, P.; Mukhopadhyay, S. Supramolecular assemblies involving anion- π and lone pair- π interactions: Experimental observation and theoretical analysis. *CrystEngComm* **2011**, *13*, 4519–4527. [[CrossRef](#)]

Disclaimer/Publisher's Note: The statements, opinions and data contained in all publications are solely those of the individual author(s) and contributor(s) and not of MDPI and/or the editor(s). MDPI and/or the editor(s) disclaim responsibility for any injury to people or property resulting from any ideas, methods, instructions or products referred to in the content.